J Ther Eng, Vol. 8, No. 1, pp. 52–66, January 2022

Journal of Thermal Engineering
Web page info: https://jten.yildiz.edu.tr
DOI: 10.18186/thermal.1067015

Journal of Thermal Engineering

Research Article

Thermoeconomic analysis and multi-objective optimization of a novel trigeneration system consisting of kalina and humidification-dehumidification desalination cycles

Pooria BEHNAM[1], Meysam FAEGH[2], Iman FAKHARI[3], Pouria AHMADI[3,*], Ehsan FAEGH[4], Marc A. ROSEN[5]

[1]School of Engineering, Edith Cowan University, 270 Joondalup Drive, Joondalup, Perth, WA 6027, Australia
[2]Department of Mechanical Engineering, Sharif University of Technology, Tehran, Iran
[3]School of Mechanical Engineering, College of Engineering, University of Tehran, Iran
[4]Department of Chemical Engineering, College of Engineering, University of Tehran, Iran
[5]Faculty of Engineering and Applied Science, University of Ontario Institute of Technology, 2000 Simcoe St. North, Oshawa, Ontario, L1G 0C5, Canada

ARTICLE INFO

Article history
Received: 28 April 2020
Accepted: 24 September 2020

Keywords:
Trigeneration, Kalina cycle, Humidification-dehumidification, Desalination, Optimization

HIGHLIGHTS

- A novel trigeneration cycle comprised of humidification-dehumidification (HDH) and Kalina cycle is proposed.
- The evaporative condenser acts as a humidifier and condenser simultaneously.
- The complexity of the Kalina-HDH cycle is reduced using the evaporative condenser.
- A detailed thermoeconomic analysis and multi-objective optimization are performed.
- The optimized exergy efficiency and total cost rate vary between 14.9–41.6% and 1.13-2.19 $/h, respectively.

ABSTRACT

Low-temperature geothermal heat sources have the highest share of geothermal energy in the world. Utilization of these heat sources for energy and freshwater generation can play an important role in meeting energy and freshwater demands. To do so, this study aims to propose a novel trigeneration cycle powered by low-temperature geothermal sources. The proposed system, which is an integration of Kalina and humidification-dehumidification (HDH) cycles, is used for the generation of electricity, heating, and freshwater. For the Kalina cycle, an evaporative condenser is used. It also acts as a humidifier and heater of the humidification-dehumidification desalination cycle, resulting in a reduction in the

***Corresponding author.**
*E-mail address: Pahmadi@ut.ac.ir

This paper was recommended for publication in revised form by Regional Editor Hafiz Muhammad Ali

Published by Yıldız Technical University Press, İstanbul, Turkey

complexity of the trigeneration system. A comprehensive thermoeconomic analysis and multi-objective optimization of the new trigeneration system are performed. First, a detailed parametric study is carried out to investigate the effects of key design parameters, including turbine inlet pressure, condenser temperature, basic solution ammonia concentration, air mass flow rate and heat source temperature, on the thermoeconomic criteria. Then, a multi-objective optimization is conducted to determine the best design parameters, considering exergy and total cost rate as the objective functions. The optimal solution Pareto frontier indicates that the exergy efficiency and total cost rate vary in the range of 14.9–41.6% and 1.13–2.19 $/*h*, respectively. Analyses of the scattered distributions of design parameters reveal that lower heat source temperatures tend to optimize the objective functions. However, altering other design parameters has a significant effect on the trade-off between exergy efficiency and total cost rate.

Cite this article as: Pooria B, Meysam F, Iman F, Pouria A, Ehsan F, Marc A. R. Thermoeconomic analysis and multi-objective optimization of a novel trigeneration system consisting of kalina and humidification-dehumidification desalination cycles. J Ther Eng 2021;8(1):52–66.

INTRODUCTION

The supply of freshwater has become a serious challenge in many regions, mainly due to industrialization and rapid population growth [1]. Desalination technologies powered by various renewable energy sources can play a key role in meeting this challenge while mitigating environmental impacts. Among the various types of thermal desalination systems, the humidification-dehumidification (HDH) process exhibits distinct advantages over commonly used technologies, including simple design, low capital, and maintenance costs and capability of being powered by low-temperature heat sources [2, 3]. Due to these positive features, a comprehensive review was conducted on HDH-based refrigeration, power generation, and desalination cycles [4]. Multi-generation technologies, including cogeneration and trigeneration, not only are beneficial for mitigating freshwater and energy demands, but also have higher efficiencies and lower operating costs than single product systems [5, 6].

Combined HDH-power systems have received increasing attention due to their important role in supplying freshwater and electricity using low-temperature heat sources, including waste heat and various renewable energies. Heretofore, the combination of an organic Rankine cycle (ORC) with various configurations of HDH systems has received more attention than other power generation technologies, mainly because of the maturity, flexibility, and reliability of ORCs [7]. Various configurations of HDH-ORC technologies with different working fluids have been studied [8, 9]. Moreover, researchers have investigated the integration of a regenerative ORC [10] and a single-extraction ORC [11] with an HDH desalination process.

Another technology suitable for power generation from low-temperature heat sources such as waste heat and some renewable energy sources is the Kalina cycle [12]. Rodríguez et al. [13] compared the thermoeconomic performance of an ORC and a Kalina cycle for power generation using low-temperature geothermal water. The Kalina cycle generated 18% more net power and had a 17.8% lower levelized electricity cost than the ORC. The Kalina cycle has been widely integrated with multi-generation cycles, mainly due to the advantages of ammonia-water over organic working fluids. Despite the advantages of the Kalina cycle, such as having a variable temperature over the boiling process and environmentally favorable characteristics, the integration of the Kalina cycle with HDH technology has not yet been investigated [4].

The common characteristic of the previous combined HDH-power systems is the existence of three main components, namely humidifier, heater, and condenser. A potential method to reduce the complexity is the use of evaporative condensers instead of conventional condensers. Evaporative condensers are widely utilized in the ammonia-water based refrigeration industry because they permit lower condensing temperatures and power consumption [14]. In this regard, the evaporative condenser not only acts as the condenser of the power cycle but also functions as the humidifier and heater of the HDH cycle, reducing the complexity of combined power-HDH technologies. Recently, the application of the evaporative condenser in an HDH desalination system was investigated by Xu et al. [15]. In this enhanced HDH system, the humidifier and dehumidifier of the HDH cycle were substituted by an evaporative condenser. It was shown that the gained output ratio of the proposed HDH cycle is significantly higher than that of conventional HDH systems, highlighting the positive effect of using an evaporative condenser for humidification and condensation processes.

As mentioned before, proposing novel combined cycles driven by low-temperature heat sources can effectively mitigate the freshwater and energy demands. This study aims to introduce a novel trigeneration cycle which is powered

by low-temperature geothermal heat sources. This novel trigeneration cycle is comprised of Kalina and HDH cycles for the generation of electricity, freshwater, and hot water. To the best of authors' knowledge, the combination of Kalina and HDH desalination cycles has not been investigated yet, and previous studies were mainly focused on combined ORC-HDH systems. Moreover, in this study, the application of the evaporative condenser in the Kalina cycle is investigated. The utilization of the evaporative condenser, which acts as humidifier and heater of the HDH desalination system, not only reduces the system complexity but also lowers the water consumption in the condensation process of the ammonia-water solution. First, the thermoeconomic performance of the system is comprehensively investigated, and the effects of key design parameters on thermoeconomic criteria are analyzed using the Engineering Equation Solver (EES) software. Finally, a multi-objective optimization based on the genetic algorithm is performed with a computer code developed in MATLAB to maximize the thermodynamic performance of the system and minimize the relevant cost. A Pareto curve is also obtained from the optimization, which shows the variation of both objective functions.

SYSTEM DESCRIPTION AND ASSUMPTION

A schematic diagram of the proposed trigeneration cycle is shown in Figure 1. The system is based on a Kalina power generation cycle and an HDH desalination cycle and produces freshwater, electricity, and heating from a low-temperature geothermal heat source. To reduce the complexity, an evaporative condenser is utilized, which integrates the Kalina cycle condenser, the humidifier, and the heater of the HDH cycle in a single unit. In this regard, a two-phase ammonia-water solution enters the evaporative condenser (state 1) and, after transferring its heat to the entering air (state 11) and saline water streams, exits as a saturated liquid (state 2). The sprayed saline water in the evaporative condenser turns the entering air (state 11) into a saturated air stream (state 12) and the saline water is then pumped back to the evaporative condenser using a circulating pump. A make-up stream of saline water (state 14) enters the evaporative condenser to compensate for the amount of water absorbed by the air stream. By rejection of heat from the saturated air to the ammonia-water solution inside the dehumidifier, freshwater is produced (state 15) and dehumidified air leaves the dehumidifier as

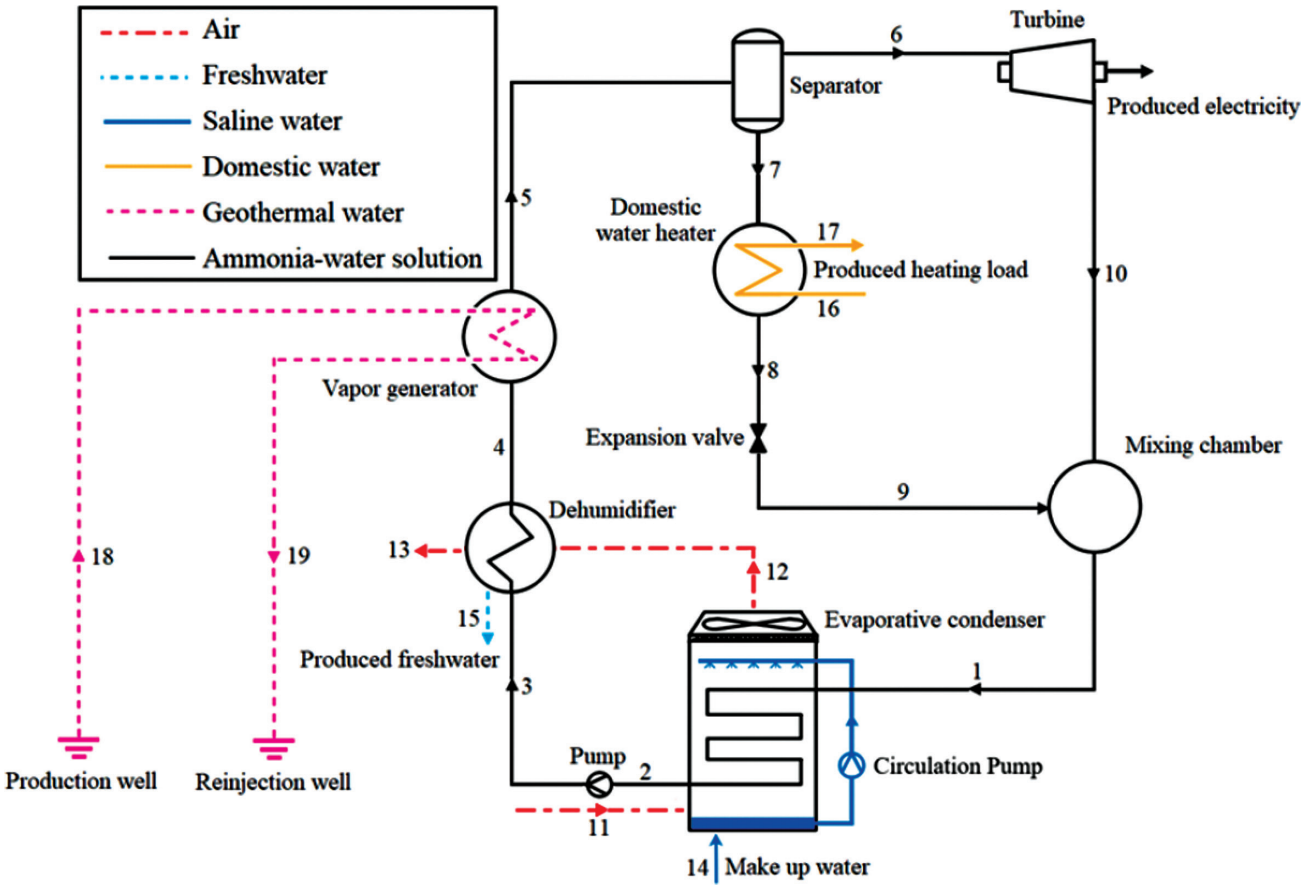

Figure 1. Schematic diagram of the proposed trigeneration system.

a saturated stream (state 13). In the vapor generator, the entering geothermal water from production well (state 18) increases the temperature of the inlet ammonia-water solution (state 4). Consequently, lower temperature geothermal water (state 19) and higher temperature two-phase ammonia-water solution (state 5) exit the vapor generator to the reinjection well and separator, respectively. The two-phase ammonia-water solution (state 5) is split into two streams: a saturated vapor (state 6) and a saturated liquid (state 7). Electricity is generated by the expansion of the saturated vapor through the turbine. Meanwhile, heating is provided in the domestic water heater, in which the inlet low-temperature domestic water (state 16) absorbs the heat removed from the incoming saturated liquid ammonia-water solution (state 7) to reach the desired domestic hot water (state 17). Finally, the liquid ammonia-water solution (state 8) exiting the domestic water heater passes through an expansion valve (state 9) and is mixed with the turbine outlet ammonia-water solution (state 10) to continue the cycle (state 1).

The following assumptions are invoked in the investigation of the proposed trigeneration system:

- The system operates under steady-state conditions.
- Pressure losses and variations in kinetic and potential energies are neglected.
- The flow passing through the expansion valve experiences an isenthalpic process.
- The ammonia-water leaving the evaporative condenser is saturated liquid [16].
- The pump and turbine both have an isenthalpic efficiency of 0.85 [17].
- Geothermal water having a mass flow rate and pressure of 3 *kg/s* and four *bar* is the heat source [10].
- In the vapor generator, the terminal temperature difference is 10°C and the pinch temperature 3°C [13].
- The vapor and liquid streams leaving the separator are saturated.
- Water at a pressure and temperature of 3 *bar* and 15°C enters the domestic water heater and, after being warmed, leaves this component at 60°C. Moreover, the terminal temperature difference is 5°C [18, 19].
- The air leaving the evaporative condenser and dehumidifier is saturated.
- The effectiveness of the dehumidifier is 0.8 [20].
- The ambient air temperature, pressure, and relative humidity are 25°C, 100 kPa, and 50%, respectively.

METHODOLOGY

Using a code developed in EES (Engineering Equation Solver), the effects of key design parameters on thermoeconomic criteria are investigated. Also, a multi-objective optimization is performed by coupling EES and MATLAB software to achieve the best performance of the trigeneration system.

Energy, Exergy and Economic Analyses

Considering each component of the proposed trigeneration system as a control volume, mass and energy balances are applied at the component level. A computer simulation code using EES software is developed to calculate the thermophysical properties of each stream so as to investigate the thermoeconomic performance of the system.

For a control volume under steady-state conditions with kinetic and potential energies neglected, mass and energy rate balance equations, as well as the exergy destruction, can be written as follows:

$$\sum \dot{m}_{in} = \sum \dot{m}_{out} \tag{1}$$

$$\sum \dot{Q} + \sum \dot{m}_{in} h_{in} = \sum \dot{W} + \sum \dot{m}_{out} h_{out} \tag{2}$$

$$\dot{I} = \sum \left(1 - \frac{T_0}{T}\right) Q + \sum \dot{E}x_{in} - \sum \dot{E}x_{out} - \dot{W} \tag{3}$$

The ammonia mass conversion is also expressible as:

$$\sum \dot{m}_{in} X_{in} = \sum \dot{m}_{out} X_{out} \tag{4}$$

An exergy analysis is carried out to investigate the performance of the trigeneration system from the perspective of the second law of thermodynamics. To calculate the total exergy of each stream, both thermophysical and chemical exergy rates are considered:

$$\dot{E}x = \dot{E}x_{Ph} + \dot{E}x_{Ch} \tag{5}$$

where the physical exergy rate is calculated as:

$$\dot{E}x_{Ph} = \dot{m}\left[(h - h_0) - T_0 (s - s_0)\right] \tag{6}$$

The chemical exergy rate is the work rate obtainable in bringing a stream of matter from the restricted dead state to the dead state reversibly, and can be written as:

$$\dot{E}x_{Ch} = \dot{m}\left[\left(\frac{x}{M_{NH_3}}\right) e^{o}_{Ch,NH_3} + \left(\frac{1-x}{M_{H_2O}}\right) e^{o}_{Ch,H_2O}\right] \tag{7}$$

Here, e^{o}_{Ch,NH_3} and e^{o}_{Ch,H_2O} denote the standard chemical exergies of ammonia and water, respectively [19, 21].

The equations used for the calculation of energy and exergy rates in each component are listed in the Table 1. Moreover, energy and exergy efficiencies are considered as thermodynamic performance criteria and are defined for the system as follows:

$$\eta_{energy} = \frac{\dot{W}_{net} + \dot{Q}_{Heating} + \dot{m}_{fw} h_{fg}}{\dot{Q}_{vapor\ generator}} \tag{8}$$

$$\eta_{\text{exergy}} = \frac{\dot{W}_{\text{net}} + \dot{E}x_{\text{Heating}} + \dot{E}x_{\text{fw}}}{\dot{E}x_{18}} \quad (9)$$

where

$$\dot{W}_{\text{net}} = \dot{m}_6 (h_6 - h_{10}) - \dot{m}_2 (h_3 - h_2) \quad (10)$$

$$\dot{Q}_{\text{Heating}} = \dot{m}_7 (h_7 - h_8) \quad (11)$$

$$\dot{Q}_{\text{vapor generator}} = \dot{m}_4 (h_5 - h_4) \quad (12)$$

$$\dot{E}x_{\text{Heating}} = \dot{E}x_{17} - \dot{E}x_{16} \quad (13)$$

$$\dot{E}x_{\text{fw}} = \dot{m}_{\text{fw}} e_{\text{ch,w}} \quad (14)$$

and where $e_{ch,w}$ in Eq. (14) denotes the specific chemical exergy of freshwater [22].

For analyzing the performance from freshwater productivity viewpoint, the gained-output-ratio (GOR) is defined as [4]:

$$\text{GOR} = \frac{\dot{m}_{\text{fw}} h_{\text{fg}}}{\dot{m}_1 (h_1 - h_2)} \quad (15)$$

Where, $\dot{m}_{fw}$ and h_{fg} represent the freshwater production rate and evaporation latent heat of desalinated water, respectively.

To investigate the proposed system from an economic viewpoint, the total cost rate is considered as the economic index and is expressed as follows [23]:

$$\dot{Z}_{\text{total}} = \sum_k \dot{Z}_k \quad (16)$$

Here, $\dot{Z}_k$ denotes the capital investment cost rate, calculated as [24]:

Table 1. Governing equations for system components

Component	Governing equations
Vapor generator	$\dot{m}_{18}(h_{18} - h_{19}) = \dot{m}_4(h_5 - h_4)$ $\dot{I}_{\text{vapor generator}} = (\dot{E}x_{18} + \dot{E}x_4) - (\dot{E}x_{19} + \dot{E}x_5)$
Water heater	$\dot{m}_7(h_7 - h_8) = \dot{m}_{16}(h_{17} - h_{16})$ $\dot{I}_{\text{water heater}} = (\dot{E}x_7 + \dot{E}x_{16}) - (\dot{E}x_8 + \dot{E}x_{17})$
Evaporative condenser	$\dot{m}_1 h_1 + \dot{m}_{11} h_{11} + \dot{m}_{14} h_{14} = \dot{m}_2 h_2 + \dot{m}_{12} h_{12}$ $\dot{m}_{14} = \dot{m}_{11}(\omega_{12} - \omega_{11})$ $\dot{I}_{\text{evaporative condenser}} = (\dot{E}x_1 + \dot{E}x_{11} + \dot{E}x_{14}) - (\dot{E}x_2 + \dot{E}x_{12})$
Dehumidifier	$\varepsilon = \max\left(\frac{h_{12} - h_{13}}{h_{12} - h_{13,\text{ideal}}}, \frac{h_4 - h_3}{h_{4,\text{ideal}} - h_3}\right)$ $h_{13,\text{ideal}} = h(\text{AirH}_2\text{O}, T_3, RH_{13}, P_{13})$ $\dot{m}_3 h_3 + \dot{m}_{12} h_{12} = \dot{m}_4 h_4 + \dot{m}_{13} h_{13} + \dot{m}_{15} h_{15}$ $\dot{I}_{\text{dehumidifier}} = (\dot{E}x_3 + \dot{E}x_{12}) - (\dot{E}x_4 + \dot{E}x_{13} + \dot{E}x_{15})$
Pump	$\dot{w}_{pump} = v_2(P_3 - P_2)/\eta_{pump}$ $\dot{I}_{\text{pump}} = (\dot{W}_{pump} + \dot{E}x_2) - \dot{E}x_3$
Turbine	$\dot{W}_{turbine} = \dot{m}_6(h_6 - h_{10})$ $\dot{I}_{\text{turbine}} = Ex_6 - (\dot{W}_{turbine} + \dot{E}x_{10})$
Separator	$\dot{m}_5 h_5 = \dot{m}_6 h_6 + \dot{m}_7 h_7$ $\dot{I}_{\text{separator}} = \dot{E}x_5 - (\dot{E}x_6 + \dot{E}x_7)$
Expansion valve	$h_8 = h_9$ $\dot{I}_{\text{expansion valve}} = (\dot{E}x_8 + \dot{E}x_9)$
Mixing chamber	$\dot{m}_9 h_9 + \dot{m}_{10} h_{10} = \dot{m}_1 h_1$ $\dot{I}_{\text{mixing chamber}} = (\dot{E}x_9 + \dot{E}x_{10}) - \dot{E}x_1$

$$\dot{Z}_k = \frac{Z_k \varphi CRF}{\tau} \quad (17)$$

where Z_k is the capital investment cost, φ is the maintenance factor which is set to 1.06, τ is annual operating hours which is set to 8000, and CRF is capital recovery factor, which is defined as [25]:

$$CRF = \frac{i(1+i)^N}{(1+i)^N - 1} \quad (18)$$

Here, *i* and *N* correspond respectively to the interest rate and the system lifetime, and are selected to be 12% and 20 years [25].

The capital investment cost (Z_k) is calculated for each component according to the expressions in Table 2, and the heat transfer area of each heat exchanger is calculated based on the LMTD (logarithmic mean temperature difference) method. The heat transfer rate for component k can be expressed as:

$$\dot{Q}_k = U_k A_k \left[\frac{(T_{h1} - T_{c2}) - (T_{h2} - T_{c1})}{Ln\left((T_{h1} - T_{c2})/(T_{h2} - T_{c1})\right)} \right] \quad (19)$$

Approximate values of the overall heat transfer coefficients of each heat exchanger in the system are listed in Table 3.

Table 2. The capital investment cost function of each component

Component	Capital investment cost function ($)	Reference
Vapor generator	$Z = 2143 \times A^{0.514}$	[26]
Water heater	$Z = 2143 \times A^{0.514}$	[26]
Evaporative condenser	$Z = 2143 \times A^{0.514}$	[26]
Dehumidifier	$Z = 2143 \times A^{0.514}$	[26]
Pump	$Z = 1120 \times \dot{w}^{0.8}$	[26]
Turbine	$Z = 4405 \times \dot{W}^{0.7}$	[27]
Separator	$Z = 280.3 \times \dot{m}_{in}^{0.67}$	[26]
Expansion valve	$Z = 114.5 \times \dot{m}_{in}$	[28]

Table 3. Overall heat transfer coefficients [29, 30]

Component	U($kW/m^2 \cdot K$)
Vapor generator	1.6
Water heater	1
Evaporative condenser	0.3
Dehumidifier	1

MULTI-OBJECTIVE OPTIMIZATION

Multi-objective optimization is a robust tool for attaining the best design parameters in energy systems exhibiting conflicting objective functions that need to be addressed simultaneously [31, 32]. In multi-objective optimization, there exists a set of optimum solutions known as the Pareto frontier, instead of the unique solution obtained from the single-objective optimization process [33]. Multi-objective optimization assists decision-makers in selecting the best design point among the set of optimal solutions according to preferences in an industrial project. In this study, a genetic algorithm is utilized in the optimization process, and exergy efficiency, as well as total cost rate, are considered as the two objective functions in the multi-objective optimization. The overall exergy efficiency considers the energy quality as well as deviations of the system from its idealized working condition. Therefore, overall exergy efficiency was preferred to energy efficiency and chosen as the objective function. Figure 2 presents the flow chart for the multi-objective optimization methodology. As can be seen, multi-objective optimization starts with the definition of design parameters and their boundaries (Table 4). By choosing the genetic algorithm properties according to Table 5, the multi-objective optimization algorithm generates the initial random population. In an iterative process, the generated population in MATLAB is evaluated based on objective functions imported from EES. More details on

Table 4. Base case condition and variation boundaries for each of the design parameters in parametric study.

Design parameter	Unit	Boundaries	References
Turbine inlet pressure (P_6)	*bar*	14–21	[17]
Heat source temperature (T_{18})	*K*	365–400	[13, 19]
Basic ammonia concentration (X_2)	–	0.6–0.7	[35]
Condenser temperature (T_2)	*K*	308–320	[19]
Air mass flow rate ($\dot{m}_a$)	kg/s	1.2–2.3	–

Table 5. Genetic algorithm properties.

Parameter	Value
Constraint tolerance	0.001
Crossover fraction	0.8 [36, 37]
Mutation fraction	0.01 [36, 37]
Function tolerance	0.0001
Maximum generations	1000
Pareto fraction	0.35
Population size	50

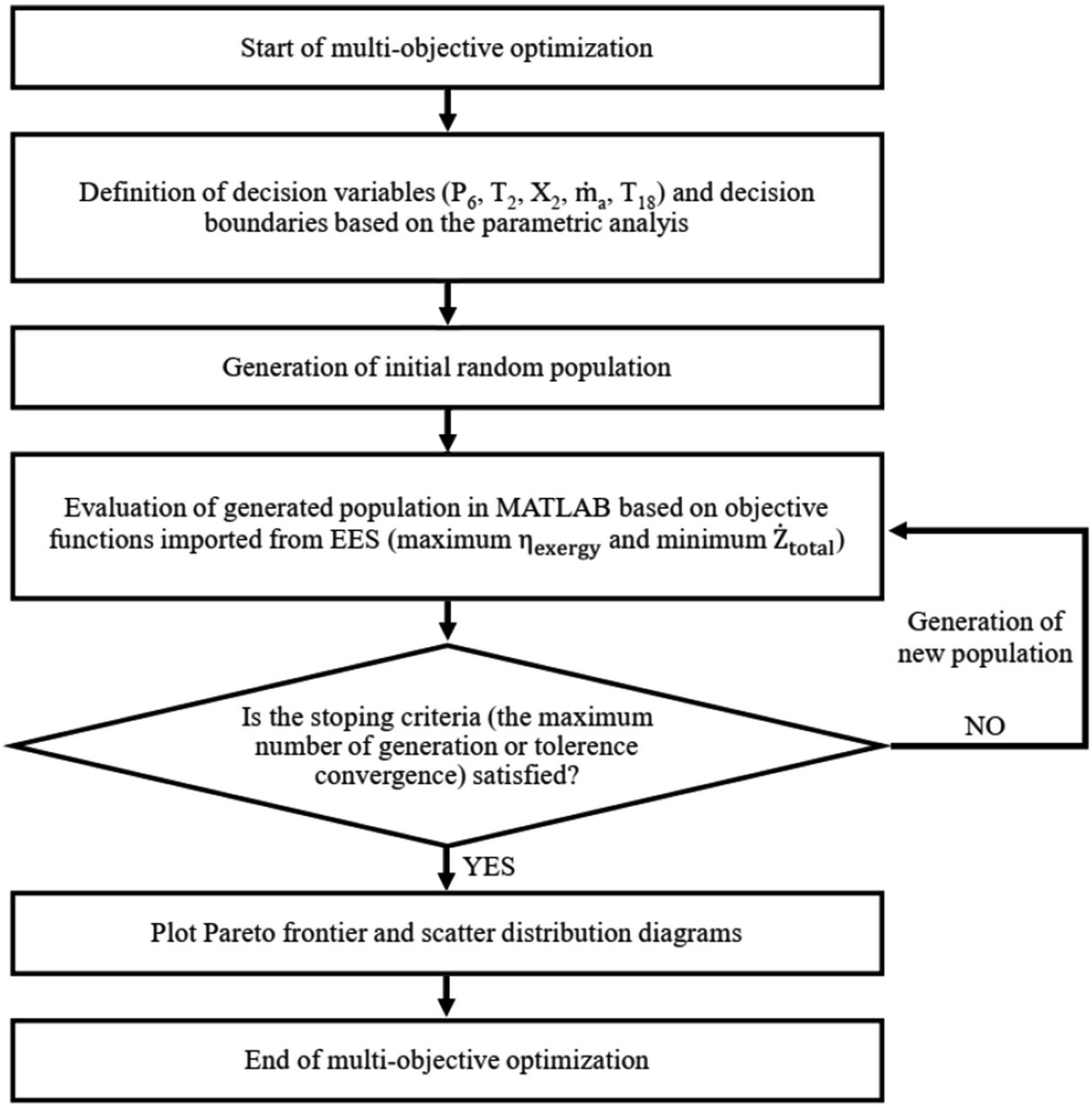

Figure 2. Flow chart of the multi-objective optimization methodology.

the genetic optimization algorithm can be found in [34]. Finally, scatter distribution diagrams for the design parameters, and the optimal solution Pareto frontier are obtained, thereby facilitating the selection of the best design point following decision maker targets.

RESULTS AND DISCUSSION

Parametric Analysis

In the parametric analysis, five key design parameters are considered: turbine inlet pressure, condenser temperature, basic solution ammonia concentration, air mass flow rate, and heat source temperature. To investigate the effects of each design parameter on the thermoeconomic performance of the system, when a parameter is changed, the others are held constant (at the base case condition). The base case condition and its corresponding thermo-physical properties for each state of the trigeneration system are given in Table 6.

For the base case condition, the energy efficiency, exergy efficiency, and total cost rate of the proposed cycle are 44.2%, 32.1%, and 1.55 \$/*h*, respectively. Also, the proposed cycle produces 21.22 *kW* of electricity, 163.8 *kW* heating, and 37.51 kg/h freshwater. The developed thermodynamic

Table 6. Thermodynamic properties of each state for the base case condition*

State	T (*K*)	P (*bar*)	h (*kJ/kg*)	X	s (*kJ/kg·K*)	ṁ (*kg/s*)	Ėx (*kW*)
1	329	9.03	373.9	0.65	1.72	0.78	10161
2	313.15	9.03	−30.07	0.65	0.46	0.78	10137
3	313.3	17	−28.82	0.65	0.46	0.78	10138
4	320.7	17	5.746	0.65	0.57	0.78	10140
5	363.15	17	610.8	0.65	2.32	0.78	10207
6	363.15	17	1456	0.98	4.61	0.27	5267
7	363.15	17	169.2	0.47	1.11	0.51	4940
8	293.1	17	−148.6	0.47	0.14	0.51	4925
9	293.3	9.03	−148.6	0.47	0.15	0.52	4925
10	334.4	9.03	1373	0.98	4.65	0.27	5242
11	298.15	1	50.67	–	5.79	1.5	0
12	322.6	1	269.8	–	6.5	1.5	12.18
13	321.1	1	250.3	–	6.44	1.5	10.12
14	298.15	1	104.8	–	0.37	0.11	0
15	321.8	1	203.9	–	0.69	0.01	0.039
16	288.15	3	63.2	–	0.22	0.87	0.8
17	333.15	3	251.4	–	0.83	0.87	7.11
18	373.15	4	419.3	–	1.31	3	102.8
19	335.4	4	261	–	0.86	3	27.91

*P_6 = 17 *bar*, T_2 = 313.15 *K*, X_2 = 0.65, 15 T_{18} = 373. *K*, $\dot{m}_a$ = 1.5 *kg/s*

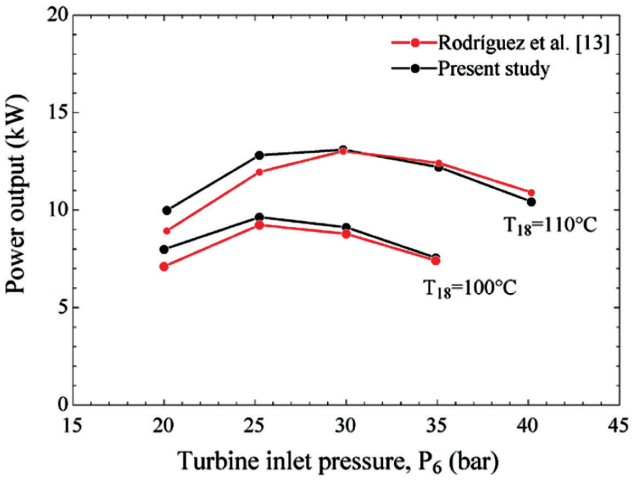

Figure 3. Variation in power output of the Kalina cycle versus turbine inlet pressure.

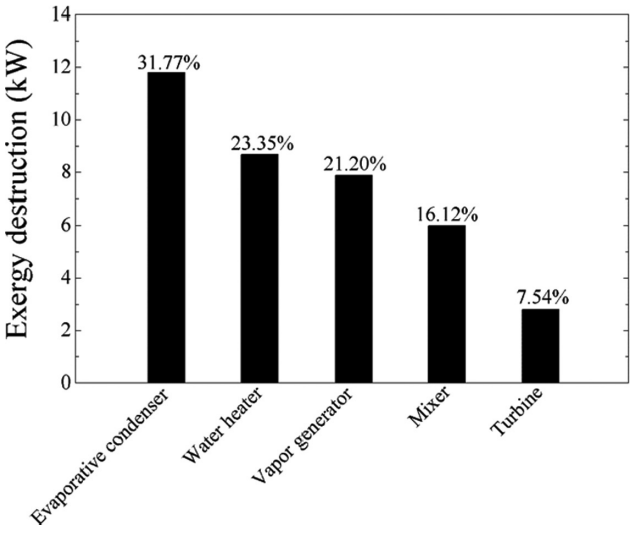

Figure 4. Exergy destruction distribution of the cycle.

model is verified using the data obtained from Rodríguez et al. [13] for a Kalina cycle driven by low-temperature geothermal water. The variation in power output with different turbine inlet pressures for two heat source temperatures (100°C and 110°C) is shown in Figure 3 There is an optimum value for inlet turbine pressure to generate the maximum power output for each heat source temperature. It can be seen that under similar working conditions ($\dot{m}_{18}$ = $1\frac{kg}{s}$, X_2 = 0.84, T_2 = 37°C), there was a favorable agreement between the obtained results from this study and those from Rodríguez et al. [13].

The exergy destruction of each component is illustrated in Figure 4.It can be seen that the evaporative condenser and water heater components had the highest

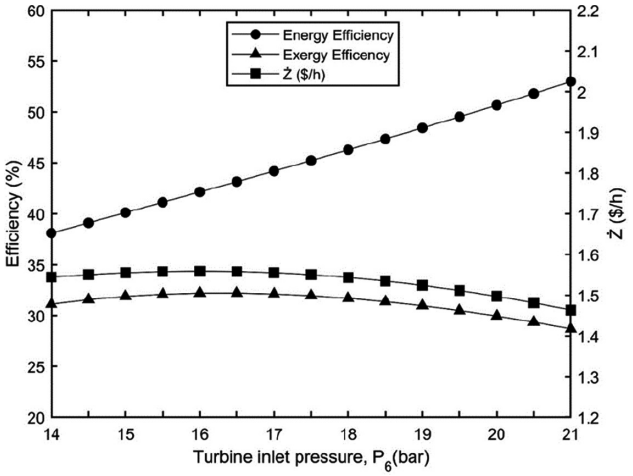

Figure 5. Variations in various thermoeconomic criteria with turbine inlet pressure.

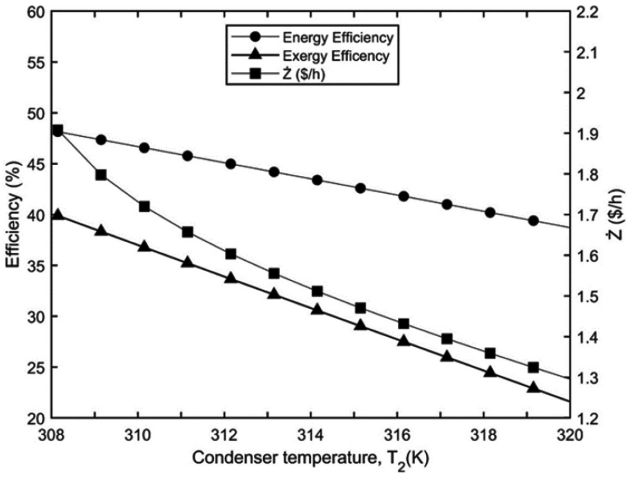

Figure 6. Variations in various thermoeconomic criteria with condenser temperature.

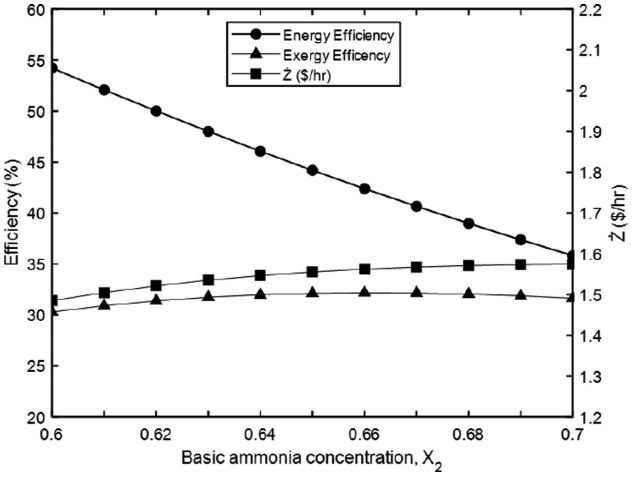

Figure 7. Variations in various thermoeconomic criteria with basic ammonia concentration.

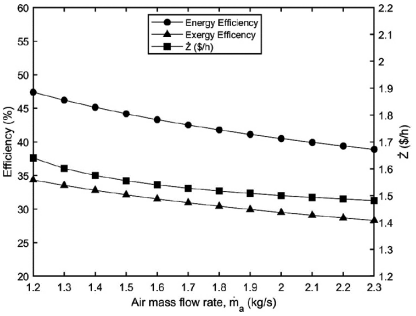

Figure 8. Variations in various thermoeconomic criteria with air mass flow rate.

irreversibilities, constituting of 31.77% and 23.35% of total exergy destruction, respectively. This highlights the need for better designing of the evaporative condenser, which can lead to enhanced exergetic performance of the cycle. It is worth mentioning that the condenser in previous combined ammonia-water cycles also had the highest share of exergy destruction [16, 38].

The effects of varying the turbine inlet pressure on energy efficiency, exergy efficiency, and total cost rate are shown in Figure 5. It is seen that the energy efficiency increases steadily with increasing turbine inlet pressure. The main reason for this is that, by increasing the turbine inlet pressure, the required input energy to the vapor generator decreases significantly. Moreover, the effect of heating load augmentation as a direct result of increasing the turbine inlet pressure is more significant than the associated decline in the generation rate of electricity and freshwater. It can be also observed that both exergy efficiency and total cost rate exhibit similar behavior as the turbine inlet pressure increases. As the turbine inlet pressure increases, the exergy efficiency and total cost rate reach a peak and then experience a downward trend. This is due to the fact that an increase in the turbine inlet pressure has an opposite effect on the exergies of heating and freshwater. That is, a rise in turbine inlet pressure leads to a decrease in freshwater exergy and an increase in heating exergy. Furthermore, the cost rates of the turbine and domestic water heater rise while those of the evaporative condenser and vapor generator decrease, leading to an optimum value for the total cost rate.

As illustrated in Figure 6, the higher is the condenser temperature; the lower are the energy and exergy efficiencies. With an increase in condenser temperature, the capacity of the evaporative condenser drops significantly, thereby lowering the production rate of freshwater. Furthermore, the total cost rate decreases considerably at higher condenser temperatures, mainly due to the decline in the cost rates of the evaporative condenser and turbine.

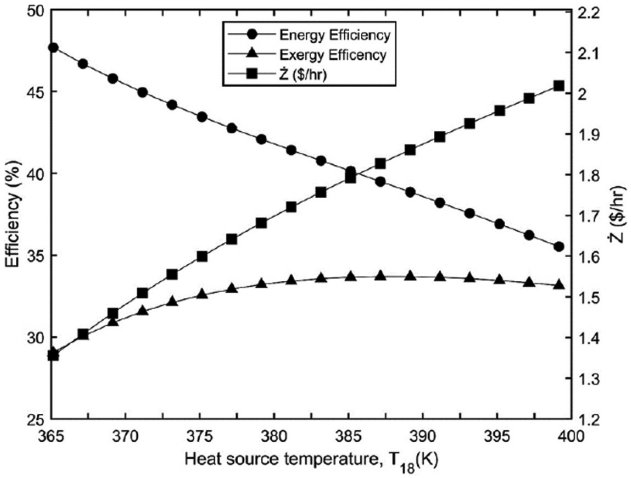

Figure 9. Variations in various thermoeconomic criteria with heat source temperature.

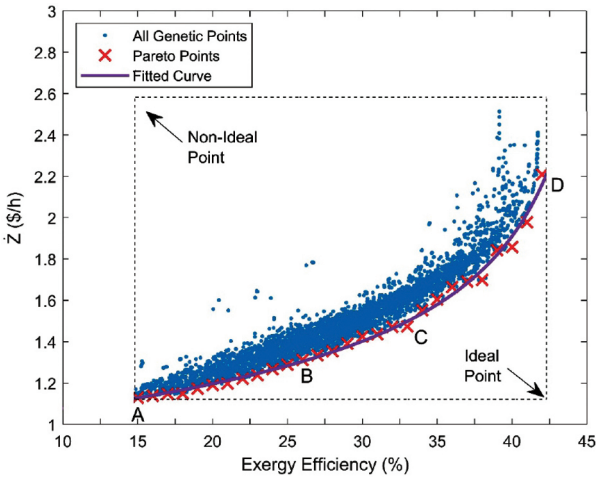

Figure 10. Distribution of optimized points and the Pareto optimal solutions for objective functions.

Table 7. Parameter values for base case and optimized conditions for points A-D.

Parameter	Base case	A	B	C	D
$P_6\,(bar)$	17	15.29	17.72	14.87	17.25
$T_2\,(K)$	313.15	319.5	316.4	312.2	308.5
X_2	0.65	0.7	0.65	0.65	0.68
$T_{18}\,(K)$	373.15	367.57	368.14	366.68	377.35
$\dot{m}_a\,(kg/s)$	1.5	2.07	1.43	1.5	1.26
$\dot{W}_{net}(kW)$	21.22	8.61	15.49	16.97	28.92
$\dot{Q}_{Heating}(kW)$	163.8	117.6	162.2	146.9	143.9
$\dot{m}_{fw}$(kg/h)	37.51	0.87	8.682	38.17	87.44
GOR	0.075	0.001	0.020	0.083	0.137
$\eta_{energy}(\%)$	44.2	25.92	44.99	42.79	43.04
$\eta_{exergy}(\%)$	32.12	14.9	25.45	32.47	41.57
$\dot{Z}_{total}(\$/h)$	1.55	1.13	1.31	1.47	2.19

Figure 7 indicates the variations in energy and exergy efficiencies and total cost rate with basic ammonia concentration. Higher basic ammonia concentrations result in lower energy efficiencies. This stems from the fact that, for fixed temperature and pressure of the two-phase ammonia-water solution entering the separator (state 5), the vapor quality increases (Q_5) by increasing the basic ammonia concentration. Therefore, the required input heat to the vapor generator rises, while the generated heating load provided by the domestic water heater decreases. An optimum value of the exergy efficiency can be attained by altering the basic ammonia concentration due to its opposite effect on the exergy of the produced freshwater and heating load. With an increase in the basic ammonia concentration, the capacity of the evaporative condenser and freshwater productivity rises. Also, increasing the basic ammonia concentration leads to larger values of the vapor generator and evaporative condenser costs, thus increasing the total cost rate.

As depicted in Figure 8, the energy and exergy efficiencies experience a downward trend with an increase in the air mass flow rate. The main reason for this is that, by increasing the air mass flow rate entering the evaporative condenser, a decrease occurs in the absolute humidity of the air entering the dehumidifier, resulting in lower freshwater productivity. Moreover, the total cost rate decreases at higher air mass flow rates due to the lower evaporative condenser cost.

Figure 9 indicates the influence of heat source temperature on several thermoeconomic criteria. As can be seen, higher heat source temperatures lead to a lower energy efficiency due to the increased input energy to the cycle. However, there exists an optimum value for heat source

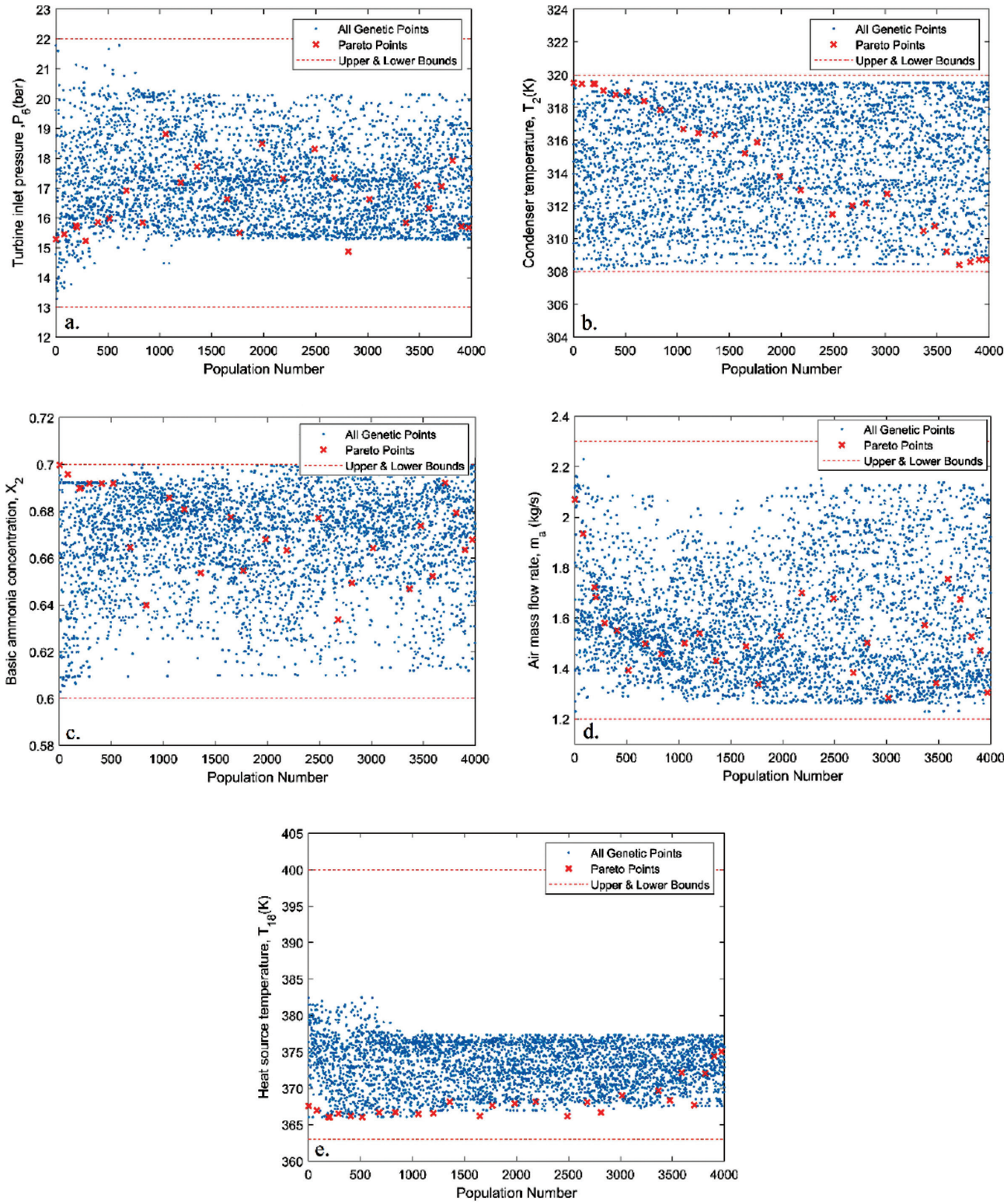

Figure 11. Scatter distributions of various design parameters with population in Pareto frontier: turbine inlet pressure (a), condenser temperature (b), basic ammonia concentration (c), air mass flow rate (d) and heat source temperature (e).

temperature that maximizes the exergy efficiency. By increasing the heat source temperature, the flow cost rates of the vapor generator and turbine rise, resulting in a significant increase in the total cost rate.

Optimization Results

As can be inferred from the parametric analysis of the proposed cycle, variations in the design parameters exhibit conflicting effects on objective functions. This highlights the importance of multi-objective optimization for achieving the best design point aligned with the priority of objective functions. Figure 10 presents all genetic points optimized in terms of exergy efficiency and total cost rate over 1000 generations. The red curve in Figure 10 represents the Pareto frontier, where a set of optimum solutions are available to design the system. As can be seen, higher values for total cost rate are required at higher exergy efficiencies. While the highest exergy efficiency occurs at point D, the total cost rate is at its maximum. This indicates that point D is the best of the optimal design points in terms of exergy efficiency. But, point A has the minimum total cost rate and exergy efficiency, providing the best optimal solution in terms of total cost rate. In multi-objective optimization, it is desirable for decision makers to reach a hypothetical ideal point where the exergy efficiency is maximized, and the total cost rate is minimized. Since it is impossible to optimize both objective functions simultaneously, the final optimal design point (for example point B or C in Figure 10), should be chosen from the Pareto frontier considering the degree of importance of both objective functions. In this study, selecting the point C as the design point seems rational, providing acceptable values of exergy efficiency and total cost rate. Table 7, shows the design parameters and thermoeconomic criteria for the base case and optimum points A-D. Points A and D are single-objective optimum solutions in terms of total cost rate and exergy efficiency, respectively. The lowest total cost rate of 1.14 \$/*h* and the highest exergy efficiency of 41.57% are considered as the solutions of single-objective optimization at points A and D, respectively. Point B, with an exergy efficiency of 25.45% and a total cost rate of 1.31 \$/*h* can be selected as the optimal design point. Also, the system could be designed at optimum point C, with a total cost rate of 1.47 \$/*h*, as well as a higher exergy efficiency (32.47%) compared to point B. To achieve a relationship between exergy efficiency and total cost rate, a curve is fitted on the optimum solution Pareto frontier as:

$$\dot{Z}_{total} = \frac{-121.6\eta_{ex}^2 + 6518\eta_{ex} + 1239}{\eta_{ex}^3 - 189.8\eta_{ex}^2 + 6882\eta_{ex} - 417.2} \qquad (20)$$

It is worth mentioning that according to Table 7, the amount of heating load is more than the power generation in the present cycle. In the case of more need for power generation, there is a possibility for the further studies on the replacement of the water heater with an ORC cycle for more generation of power. As can be seen from Table 7, design parameters at optimum points experience a scattered distribution within their boundaries. To better highlight the variations of design parameters during the optimization process, scattered distribution diagrams are shown in Figure 11. It can be inferred from Figure 11 (a-d) that the turbine inlet pressure (P_6), condenser temperature (T_2), basic ammonia concentration (X_2) and air mass flow rate ($\dot{m}_a$) each have a scattered distribution among their examined boundaries. This illustrates that these design parameters have conflicting effects on improving the exergy efficiency and total cost rate. However, as depicted in Figure 11 (e), heat source temperature (T_{18}) exhibits a different behavior and tends to be as low as possible at the optimum points. Furthermore, decreasing the heat source temperature enhances both of the objective functions. It is worth mentioning that the ranges in Figure 11 are considered with a margin of 10–15% to cover the all possible operation points of the system [23, 39].

CONCLUSION

A novel trigeneration system comprised of Kalina and humidification-dehumidification desalination cycle is investigated from thermoeconomic a viewpoint. The proposed cycle benefits from an evaporative condenser, which not only cools the temperature of the ammonia-water solution in the Kalina cycle, but also acts as the humidifier and heater of the humidification-dehumidification desalination cycle. Therefore, system complexity decreases by substituting the three mentioned components with an evaporative condenser. A thermoeconomic analysis and multi-objective optimization are performed, and the effects of design parameters on system performance are studied. The following conclusions can be drawn from the results:

- Increasing the turbine inlet pressure causes the energy efficiency to rise continuously, while exergy efficiency and total cost rate take on optimum values.
- Energy and exergy efficiencies and total cost rate decrease as air mass flow rates and condenser temperatures rise.
- A higher basic ammonia concentration results in lower energy efficiency and higher total cost rate. Moreover, the exergy efficiency reaches a peak and then experiences a downward trend as the basic ammonia concentration rises.
- With an increase in heat source temperature, energy efficiency declines, but exergy efficiency and total cost rate rise.
- In the multi-objective optimization, a curve is fitted on the optimal solution Pareto frontier, indicating the relationship between exergy efficiency and total cost rate. It can be seen from the Pareto frontier that an

increase of 118% in exergy efficiency can be attained only by a 30% rise in total cost rate.

- The optimization results show that the turbine inlet pressure, condenser temperature, basic ammonia concentration, and air mass flow rate each exhibit a scattered distribution within their examined boundaries, indicating that they have a significant impact on the trade-off between objective functions. However, declining heat source temperatures tend to increase the exergy efficiency and decrease the total cost rate.

NOMENCLATURE

A	area (m^2)
CRF	capital recovery factor
e	standard chemical exergy (kJ/kg)
$\dot{E}x$	exergy flow rate (kW)
GOR	gained-output-ratio
h	specific enthalpy (kJ/kg)
HDH	humidification-dehumidification
I	interest rate (%)
$\dot{i}$	Exergy destruction (kW)
LMTD	logarithmic mean temperature difference (K)
M	molar mass (g/mol)
$\dot{m}$	mass flow rate (kg/s)
N	system lifetime ($year$)
ORC	organic Rankine cycle
P	pressure (bar)
$\dot{Q}$	heat transfer rate (kW)
s	specific entropy ($kJ/kg, K$)
T	temperature (K)
U	overall heat transfer coefficient ($kW/m^2, K$)
v	Specific volume (m^3/kg)
$\dot{W}$	Work rate (kW)
X	ammonia mass fraction
Z	capital investment cost ($)
$\dot{Z}$	total cost rate ($/h$)

Greek letter

η	efficiency
τ	annual operating hours
φ	maintenance factor

Subscripts

0	Dead state
A	air
C	cold stream
Ch	chemical
fw	freshwater
H_2O	water
In	inlet
NH_3	ammonia
out	outlet
Ph	physical

AUTHORSHIP CONTRIBUTIONS

Authors equally contributed to this work.

DATA AVAILABILITY STATEMENT

The authors confirm that the data that supports the findings of this study are available within the article. Raw data that support the finding of this study are available from the corresponding author, upon reasonable request.

CONFLICT OF INTEREST

The author declared no potential conflicts of interest with respect to the research, authorship, and/or publication of this article.

ETHICS

There are no ethical issues with the publication of this manuscript.

REFERENCES

[1] Xiao G, Wang X, Ni M, Wang F, Zhu W, Luo Z, et al. A review on solar stills for brine desalination. Appl Energy 2013;103:642-652. [CrossRef]

[2] Narayan GP, Sharqawy MH, Summers EK, Lienhard JH, Zubair SM, Antar MA. The potential of solar-driven humidification–dehumidification desalination for small-scale decentralized water production. Renew Sust Energy Rev 2010;14:1187-1201. [CrossRef]

[3] Behnam P, Shafii MB. Examination of a solar desalination system equipped with an air bubble column humidifier, evacuated tube collectors and thermosyphon heat pipes. Desalination 2016;397:30-37. [CrossRef]

[4] Faegh M, Behnam P, Shafii MB. A review on recent advances in humidification-dehumidification (HDH) desalination systems integrated with refrigeration, power and desalination technologies. Energy Convers Manag 2019;196:1002-1036. [CrossRef]

[5] Parikhani T, Azariyan H, Behrad R, Ghaebi H, Jannatkhah J. Thermodynamic and thermoeconomic analysis of a novel ammonia-water mixture combined cooling, heating, and power (CCHP) cycle. Renew Energy 2020;145:1158-1175. [CrossRef]

[6] Takleh HR, Zare V. Employing thermoelectric generator and booster compressor for performance improvement of a geothermal driven combined power and ejector-refrigeration cycle. Energy Convers Manag 2019;186:120-130. [CrossRef]

[7] Zare V. A comparative exergoeconomic analysis of different ORC configurations for binary geothermal power plants. Energy Convers Manag 2015;105:127-138. [CrossRef]
[8] Yari M, Ariyanfar L, Aghdam EA. Analysis and performance assessment of a novel ORC based multigeneration system for power, distilled water and heat. Renew Energy 2018;119:262-281. [CrossRef]
[9] Ariyanfar L, Yari M, Aghdam EA. Proposal and performance assessment of novel combined ORC and HDD cogeneration systems. Appl Therm Eng 2016;108:296-311. [CrossRef]
[10] He WF, Han D, Wen T. Energy, entropy and cost analysis of a combined power and water system with cascade utilization of geothermal energy. Energy Convers Manag 2018;174:719-729. [CrossRef]
[11] He WF, Wu F, Kong YP, Wen T, Chen JJ, Han D. Parametric analysis of a power-water cogeneration system based on single-extraction organic Rankine cycle. Appl Therm Eng 2019;148:382-390. [CrossRef]
[12] Zhang X, He M, Zhang Y. A review of research on the Kalina cycle. Renew Sust Energy Rev 2012;16:5309-5318. [CrossRef]
[13] Campos Rodríguez CE, Escobar Palacio JC, Venturini OJ, Silva Lora EE, Cobas VM, Marques dos Santos D, et al. Exergetic and economic comparison of ORC and Kalina cycle for low temperature enhanced geothermal system in Brazil. Appl Therm Eng 2013;52:109-119. [CrossRef]
[14] Stoecker WF. Industrial refrigeration handbook: McGraw-Hill, 1998.
[15] Xu H, Sun XY, Dai YJ. Thermodynamic study on an enhanced humidification-dehumidification solar desalination system with weakly compressed air and internal heat recovery. Energy Convers Manag 2019;181:68-79. [CrossRef]
[16] Behnam P, Faegh M, Shafii MB. Thermodynamic analysis of a novel combined power and refrigeration cycle comprising of EKalina and ejector refrigeration cycles. Int J Refrig 2019;104:291-301.
[17] Ghaebi H, Parikhani T, Rostamzadeh H, Farhang B. Thermodynamic and thermoeconomic analysis and optimization of a novel combined cooling and power (CCP) cycle by integrating of ejector refrigeration and Kalina cycles. Energy 2017;139:262-276. [CrossRef]
[18] Ahmadi P, Dincer I, Rosen MA. Exergo-environmental analysis of an integrated organic Rankine cycle for trigeneration. Energy Convers Manag 2012;64:447-453. [CrossRef]
[19] Yari M, Mehr AS, Zare V, Mahmoudi SMS, Rosen MA. Exergoeconomic comparison of TLC (trilateral Rankine cycle), ORC (organic Rankine cycle) and Kalina cycle using a low grade heat source. Energy 2015;83:712-722. [CrossRef]
[20] He WF, Zhang XK, Han D, Gao L. Performance analysis of a water-power combined system with air-heated humidification dehumidification process. Energy 2017;130:218-227. [CrossRef]
[21] Misra RD, Sahoo PK, Gupta A. Thermoeconomic evaluation and optimization of an aqua-ammonia vapour-absorption refrigeration system. Int J Refrig 2006;29:47-59. [CrossRef]
[22] Sadeghi M, Yari M, Mahmoudi SMS, Jafari M. Thermodynamic analysis and optimization of a novel combined power and ejector refrigeration cycle – Desalination system. Appl Energy 2017;208:239-251. [CrossRef]
[23] Ahmadi P, Dincer I, Rosen MA. Thermodynamic modeling and multi-objective evolutionary-based optimization of a new multigeneration energy system. Energy Convers Manag 2013;76:282-300. [CrossRef]
[24] Boyaghchi FA, Safari H. Parametric study and multi-criteria optimization of total exergetic and cost rates improvement potentials of a new geothermal based quadruple energy system. Energy Convers Manag 2017;137:130-141. [CrossRef]
[25] Mehrpooya M, Mousavi SA. Advanced exergoeconomic assessment of a solar-driven Kalina cycle. Energy Convers Manag 2018;178:78-91. [CrossRef]
[26] Mosaffa AH, Hasani Mokarram N, Garousi Farshi L. Thermoeconomic analysis of a new combination of ammonia/water power generation cycle with GT-MHR cycle and LNG cryogenic exergy. ApplTherm Eng 2017;124:1343-1353. [CrossRef]
[27] Zare V, Mahmoudi SMS, Yari M. On the exergoeconomic assessment of employing Kalina cycle for GT-MHR waste heat utilization. Energy Convers Manag 2015;90:364-374. [CrossRef]
[28] Ghaebi H, Namin AS, Rostamzadeh H. Exergoeconomic optimization of a novel cascade Kalina/Kalina cycle using geothermal heat source and LNG cold energy recovery. J Clean Product 2018;189:279-296. [CrossRef]
[29] Akbari Kordlar M, Mahmoudi SMS. Exergeoconomic analysis and optimization of a novel cogeneration system producing power and refrigeration. Energy Convers Manag 2017;134:208-220. [CrossRef]
[30] Liu H, Zhou Q, Liu Y, Wang P, Wang D. Experimental study on cooling performance of air conditioning system with dual independent evaporative condenser. Int J Refrig 2015;55:85-92. [CrossRef]
[31] Sadeghi M, Chitsaz A, Mahmoudi S, Rosen MA. Thermoeconomic optimization using an evolutionary algorithm of a trigeneration system driven by a solid oxide fuel cell. Energy 2015;89:191-204. [CrossRef]

[32] Eftekhari B, Aliehyaei M. Optimization of a new configuration of power tri-generation cycle by the use of a multi-purpose genetic algorithm. J Therm Eng 2020;6:65-91. [CrossRef]

[33] Shirazi A, Taylor RA, Morrison GL, White SD. A comprehensive, multi-objective optimization of solar-powered absorption chiller systems for air-conditioning applications. Energy Convers Manag 2017;132:281-306. [CrossRef]

[34] Ghaffarizadeh A, Ahmadi K, Flann NS. Sorting unsigned permutations by reversals using multi-objective evolutionary algorithms with variable size individuals. Conference Sorting unsigned permutations by reversals using multi-objective evolutionary algorithms with variable size individuals. IEEE Congress on Evolutionary Computation. 2011:292-295. [CrossRef]

[35] Ghaebi H, Parikhani T, Rostamzadeh H, Farhang B. Proposal and assessment of a novel geothermal combined cooling and power cycle based on Kalina and ejector refrigeration cycles. Appl Therm Eng 2018;130:767-781. [CrossRef]

[36] Hassanat A, Almohammadi K, Alkafaween E, Abunawas E, Hammouri A, Prasath V. Choosing mutation and crossover ratios for genetic algorithms—a review with a new dynamic approach. Information 2019;10:390. [CrossRef]

[37] Ahmadi P, Dincer I, Rosen MA. Exergy, exergoeconomic and environmental analyses and evolutionary algorithm based multi-objective optimization of combined cycle power plants. Energy 2011;36:5886-5898. [CrossRef]

[38] Wang J, Wang J, Zhao P, Dai Y. Thermodynamic analysis of a new combined cooling and power system using ammonia–water mixture. Energy Convers Manag 2016;117:335-342. [CrossRef]

[39] Behzadi A, Gholamian E, Houshfar E, Habibollahzade A. Multi-objective optimization and exergoeconomic analysis of waste heat recovery from Tehran's waste-to-energy plant integrated with an ORC unit. Energy 2018;160:1055-1068. [CrossRef]